



Cite this: *Soft Matter*, 2019, 15, 744

Dynamics and structure of colloidal aggregates under microchannel flow†

Ming Han, ^a Jonathan K. Whitmer ^b and Erik Lijten ^{*bcd}

The kinetics of colloidal gels under narrow confinement are of widespread practical relevance, with applications ranging from flow in biological systems to 3D printing. Although the properties of such gels under uniform shear have received considerable attention, the effects of strongly nonuniform shear are far less understood. Motivated by the possibilities offered by recent advances in nano- and microfluidics, we explore the generic phase behavior and dynamics of attractive colloids subject to microchannel flow, using mesoscale particle-based hydrodynamic simulations. Whereas moderate shear strengths result in shear-assisted crystallization, high shear strengths overwhelm the attractions and lead to melting of the clusters. Within the transition region between these two regimes, we discover remarkable dynamics of the colloidal aggregates. Shear-induced surface melting of the aggregates, in conjunction with the Plateau–Rayleigh instability and size-dependent cluster velocities, leads to a cyclic process in which elongated threads of colloidal aggregates break up and reform, resulting in large crystallites. These insights offer new possibilities for the control of colloidal dynamics and aggregation under confinement.

Received 15th July 2018,
Accepted 19th December 2018

DOI: 10.1039/c8sm01451e

rsc.li/soft-matter-journal

1 Introduction

Colloidal gelation plays an important role in the creation of wide classes of materials, resulting in stable nonequilibrium aggregates of (sub)micron-sized particles that may be deformed by modest stress. The mechanical properties of such gels are related to their internal structure. Small clusters formed during the early stages of colloidal aggregation already lack the mobility to efficiently adjust their positions. As a result, they become dynamically arrested and percolate in disordered, loose networks¹ that are firm in a quiescent environment but floppy under shear. Colloidal gels have attracted considerable attention as a model system for kinetic arrest;^{1–4} gelation has been exploited to generate porous patterns for tissue engineering scaffolds⁵ and to synthesize gel-based ink for three-dimensional (3D) printing.⁶ Moreover, when exposed to external driving forces, these gels can display a variety of remarkable behaviors, both in morphology and in dynamics. Examples include shear-induced aggregation,⁷ crystallization⁸ and melting⁹ as well as shear thinning^{10,11} and thickening.¹² Most of these phenomena have

been studied separately under ideal conditions, with uniform shear and localized particle motion, typically induced by the relative motion of two parallel boundaries. However, in many realistic applications colloidal gels are driven by a flow through confined geometries, necessarily coupling nonuniform shear and directional hydrodynamic forces.

One ubiquitous example is the flow of colloidal dispersions through a microchannel, as realized in the transport of red blood cells in a microcapillary¹³ and the pumping of ink for 3D printing through a slot channel.^{6,14} This has motivated recent attempts to explore the diffusion of individual colloids subject to a channel flow.^{15,16} Developments in nano- and microfluidics^{17–20} and in particular corresponding applications in particle assembly^{21–23} further reinforce the need to understand aggregation of (sub)microscopic particles driven within narrow confinements. Nonuniformity of shear effects exerted by flow is established at length scales comparable to the channel cross-section. In macroscopic channels, colloidal clusters are typically small compared to this scale and hence different clusters experience different shear strengths depending on their location within the channel. By contrast, clusters within a (sub)microchannel can have sizes comparable to the channel cross-section and thus different shear forces are exerted simultaneously on each individual cluster. Meanwhile, the global flow causes additional rheological effects on the aggregates, including jamming, merging, and densification.²⁴ Conversely, the presence of clusters leads to considerable disturbances of the flow profile. This rich combination of factors makes the behavior of attractive colloids under microchannel flow an interesting topic of practical relevance, which we

^a Graduate Program in Applied Physics, Northwestern University, Evanston, Illinois 60208, USA

^b Department of Materials Science and Engineering, Northwestern University, Evanston, Illinois 60208, USA. E-mail: lijten@northwestern.edu

^c Department of Engineering Sciences and Applied Mathematics, Northwestern University, Evanston, Illinois 60208, USA

^d Department of Physics and Astronomy, Northwestern University, Evanston, Illinois 60208, USA

† Electronic supplementary information (ESI) available. See DOI: 10.1039/c8sm01451e

pursue here *via* mesoscale particle-based hydrodynamic simulations. We find that the colloids, which display gel-like behavior under resting conditions,²⁵ undergo shear-assisted crystallization. Remarkably, not only does the degree of ordering depend sensitively on the flow conditions, but the order is also attained through a cyclic process in which colloidal aggregates repeatedly break up and merge again.

This paper is organized as follows. First, we provide a detailed description of our simulation model in Section 2. After demonstrating the nonuniform shear of a microchannel flow in Section 3.1, we discuss its effect on the phase behavior of a colloidal gel in Section 3.2. In Sections 3.3 and 3.4, we show that the nonuniform shear also leads to a unique rheology as well as the Plateau–Rayleigh instability for colloidal aggregates. Lastly, we conclude the paper with a brief summary in Section 4.

2 Method and model

We employ molecular dynamics (MD) simulations to model a colloidal suspension being pumped through a narrow channel. The suspension contains monodisperse colloids with diameter σ_c and volume fraction $\phi_c = 0.054$. The colloids interact *via* strong short-range attractions mediated by nonabsorbing polymers, whose presence is implicitly modeled by an Asakura–Oosawa (AO) potential^{26,27} between the colloids,

$$U_{\text{AO}}(r) = -k_{\text{B}}T\phi_{\text{p}}\left(\frac{1+\zeta}{\zeta}\right)^3\left[1 - \frac{3r/\sigma_c}{2(1+\zeta)} + \frac{1}{2}\left(\frac{r/\sigma_c}{1+\zeta}\right)^3\right],$$

$$\sigma_c \leq r \leq (1+\zeta)\sigma_c, \quad (1)$$

where ϕ_{p} is the volume fraction of the implicit polymers and ζ denotes the size ratio between the polymers and the colloids. To avoid discontinuity in forces, the AO potential is rounded with a quadratic function near the colloidal surface,²⁸

$$U_{\text{att}}(r) = \begin{cases} B(r-\sigma)^2 + C, & 0 \leq r < (1+\alpha\zeta)\sigma_c \\ U_{\text{AO}}(r) & (1+\alpha\zeta)\sigma_c \leq r \leq (1+\zeta)\sigma_c \end{cases} \quad (2)$$

with parameter $\alpha = 0.1$. The constants B and C are set to maintain the continuity of both U_{att} and its first derivative at the crossover point $r_{\text{m}} = (1+\alpha\zeta)\sigma_c$,

$$B = \frac{3k_{\text{B}}T\phi_{\text{p}}}{4\alpha\zeta^4\sigma_c^2}[(1+\zeta)^2 - (1+\alpha\zeta)^2], \quad (3)$$

$$C = U_{\text{AO}}(r_{\text{m}}) - B\alpha^2\zeta^2\sigma_c^2. \quad (4)$$

The excluded-volume effect of the colloids is implemented by a soft-core repulsion,

$$U_{\text{rep}}(r) = k_{\text{B}}T\left[\left(\frac{\sigma_c}{r}\right)^{18} - \left(\frac{1}{1+\zeta}\right)^{18}\right]^2, \quad r \leq (1+\zeta)\sigma_c, \quad (5)$$

which has the advantage that it permits direct force calculations (unlike the hard-core potential typically employed in Monte Carlo simulations). In our system, $\zeta = 0.072$ and $\phi_{\text{p}} = 0.45$ are

chosen, yielding an overall interaction with range $\Delta r_c = \zeta\sigma_c < 0.1\sigma_c$ and strength $E_b = -8k_{\text{B}}T$. This ensures the system resides within the coexistence region and therefore crystallization would occur if the system could attain equilibrium. Given its short-ranged nature, the precise form of the interaction is immaterial to the phase behavior.^{1,29}

The colloids are embedded in a solvent with kinematic viscosity $\nu \sim 4\sigma_c^2/\tau$ (where $\tau = \sqrt{m_c\sigma_c^2/k_{\text{B}}T}$ is the colloidal diffusion time, m_c the colloidal mass). The entire suspension is pumped by a pressure gradient through a narrow channel of cross-sectional dimensions $W \times W$, with W ranging from $4\sigma_c$ to $15\sigma_c$. Periodic boundary conditions are applied on the inlet and the outlet. A long channel of length $L = 80\sigma_c$, containing 132 to 1850 colloids (depending on W), is employed to avoid artifacts due to the periodicity.

To include both thermal and hydrodynamic effects, we couple our system to a multi-particle collision³⁰ (MPC) hydrodynamic solver with Andersen thermostat. The system is divided into a 3D grid with resolution $N_x \times N_y \times N_z$, with $N_x = N_y = 4(W/\sigma_c)$ and $N_z = 4(L/\sigma_c)$, for a total of 81 920 to 1 152 000 cells. Each cubic cell (linear size a_0) on average contains five point-like fluid particles with mass $m = 0.004m_c$, which exchange momentum with nearby colloids. This yields a solvent comprised of 4.096×10^5 to 5.76×10^6 fluid particles. The pressure gradient is implemented *via* a constant force acting on each fluid particle. To avoid spurious (additional) depletion forces induced by the fluid particles, we set $\sigma_c = 4.3a_0$ whereas the colloid-fluid radius is set to $\sigma_{\text{cf}} = 2a_0$, as suggested by previous work on colloidal gelation.^{31,32} The MD time step is set to $2 \times 10^{-4}\tau$ and the fluid collision step size to $2 \times 10^{-2}\tau$. The mass density of the fluid particles ρ_f gives rise to a dynamic viscosity $\mu = \rho_f\nu \sim 5.12m_c/\tau\sigma_c$. All hydrodynamic surfaces, *i.e.*, channel walls and colloidal surfaces, impose stick boundary conditions on the fluid and are treated *via* the bounce-back approach.³³ The colloid-wall and fluid-wall interactions are modeled by purely repulsive shifted-truncated Lennard-Jones potentials. The Reynolds number $\text{Re} = U_0W/\nu$ (where U_0 is the flow velocity at the centerline and W the channel width) characterizing the channel flow ranges from 10^{-3} to 10. All runs are performed for 2×10^7 MD steps (4000τ), and repeated 30-fold for each flow strength.

3 Results

3.1 Shear flow

In the absence of dispersed particles, the microchannel flow $U(x,y)$ decays from its maximum U_0 at the center to zero at the channel walls (Fig. 1a) whereas the opposite occurs to the resultant shear rate $\dot{\gamma}$ (Fig. 1b). This resembles the parabolic profile characteristic of Poiseuille flow,^{34,35} albeit distorted near the walls owing to the square cross-section.

The shear exerted by this flow results in an effective force F_s that tends to separate any two bonded colloids, imparting them with a potential energy $E_s = F_s\Delta r_c$. Specifically, for a local shear rate $\dot{\gamma}$, two bonded colloids (assuming their bond vector to be aligned perpendicular to the channel axis) are driven by flows

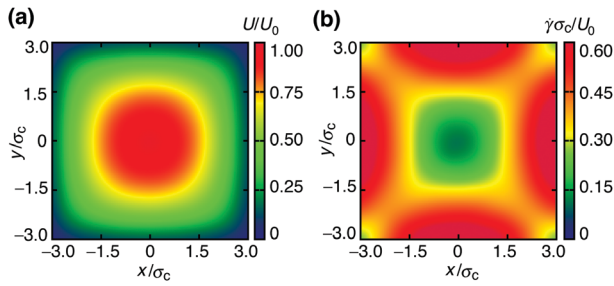


Fig. 1 Profiles of Poiseuille flow and resultant shear rate in a square channel. (a) Cross-sectional distribution of the flow speed U , normalized by the maximum speed U_0 at the channel centerline. (b) Cross-sectional distribution of the resultant shear rate $\dot{\gamma} = |\nabla_{xy}U|$, where ∇_{xy} denotes the gradient within the plane of the channel cross-section.

with velocity difference $\Delta U \sim \dot{\gamma}\sigma_c$. The resulting difference in hydrodynamic forces leads to an effective separation force $F_s \sim c_d\Delta U$ (with drag coefficient $c_d = 3\pi\mu_0\sigma_c$ for a spherical particle, where μ_0 is the fluid viscosity). We parametrize the competition between the global shear forces and the colloidal attractions by the ratio $\delta \equiv \langle E_s \rangle / E_b$. Since the average magnitude of the shear rate $\langle \dot{\gamma} \rangle$ is approximately $2U_0/W$ (due to the symmetry of the channel flow), we estimate δ as $\langle E_s \rangle / E_b = \langle F_s \rangle \Delta r_c / E_b = 6\pi\mu_0 U_0 \sigma_c^2 \Delta r_c / W E_b$. A similar definition has been proposed in the study of the pre-shear effects on colloidal gels.³⁶

3.2 Phase behavior

To study the influence of shear on ordering and crystallization, we explore a wide range of flow strengths, with δ spanning over three decades. In thermal equilibrium, strongly attractive colloids often crystallize into polymorphic patterns comprised of hexagonal close-packed (HCP) and face-centered cubic (FCC) structures,³⁷ due to their marginal difference in free energy. Thus, when determining the degree of crystallization, we take into account both structures, which we identify by computing the bond order parameters^{38,39} q_4 and w_4 for each colloid i ,

$$q_4(i) = \sqrt{\frac{4\pi}{9} \sum_{m=-4}^4 |q_{4m}(i)|^2}, \quad (6)$$

$$w_4(i) = \left(\sum_{m=-4}^4 |q_{4m}(i)|^2 \right)^{-3/2} \times \sum_{m_1+m_2+m_3=0} \begin{pmatrix} 4 & 4 & 4 \\ m_1 & m_2 & m_3 \end{pmatrix} q_{4m_1}(i) q_{4m_2}(i) q_{4m_3}(i), \quad (7)$$

where $q_{4m}(i) = [1/N_b(i)] \sum_{j=1}^{N_b(i)} Y_{4m}(\theta(\mathbf{r}_{ij}), \phi(\mathbf{r}_{ij}))$, with $N_b(i)$ the number of nearest neighbors of colloid i , $Y_{4m}(\theta, \phi)$ the spherical harmonics and $\theta(\mathbf{r}_{ij})$ and $\phi(\mathbf{r}_{ij})$ the polar angles of the bond vector $\mathbf{r}_{ij} = \mathbf{r}_i - \mathbf{r}_j$. Once the system has reached a steady state, we record a histogram of (q_4, w_4) and compute the extent of crystallization f_{crystal} from the cumulative weight of the values corresponding to FCC and HCP domains.

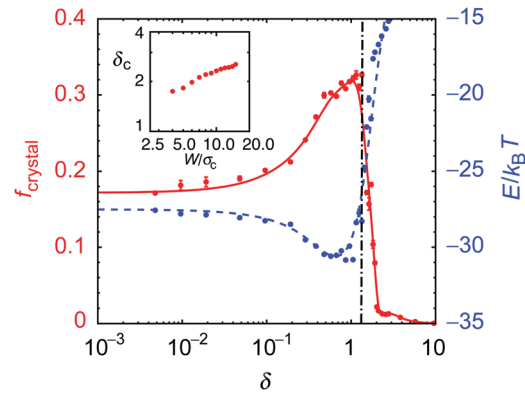


Fig. 2 Ordering and melting under shear flow. The crystal fraction f_{crystal} (solid red curve) of a colloidal suspension in a channel with $6 \times 6\sigma_c^2$ cross-section is shown as a function of the competition between global shear and colloidal attraction, characterized by δ . Moderate shear forces assist the crystallization, nearly doubling f_{crystal} for $\delta = 1$ compared to the quiescent state ($\delta = 0$). However, stronger flow results in shear-induced melting for $1 \lesssim \delta \lesssim 2$. The dashed blue curve represents the corresponding variation in the internal energy E per colloid. Inset: Dependence of the complete melting point δ_c on the channel width on a log–log scale.

Fig. 2 summarizes the degree of ordering as a function of global shear strength. In the quiescent case, owing to strong short-range attractions,⁴⁰ colloids form gel-like clusters with only small crystal nuclei, resulting in a low degree of ordering, $f_{\text{crystal}} \approx 17\%$. Application of weak shear ($\delta \lesssim 10^{-2}$) barely affects the colloidal aggregates. As δ is increased to 10^{-1} , shear effects start to overcome the kinetic arrest and assist crystallization, leading to a more ordered system. Consistent with this, the system displays a concomitant decrease in the internal energy E . Once δ exceeds 1, *i.e.*, $\langle E_s \rangle > |E_b|$, the shear forces are sufficiently strong to not merely rearrange colloidal pairs, but to fully break colloidal bonds. Such shear-induced crystallization and melting are expected.^{8,9} However, rather than displaying a discrete transition as observed in an oscillatory shearing system,⁹ here the system exhibits a melting range, $1 \lesssim \delta \lesssim 2$. This can be attributed to the nonuniformity of the shear shown in Fig. 1b: weak at the center but strong near the walls. As a consequence, within the melting range, clusters crystallize at their core but melt at their surfaces. One may further understand this regime by appealing to the particle Péclet number,

$$\text{Pe} = \frac{c_d U_0 \sigma_c}{2k_B T} = \frac{\delta E_b W}{2k_B T \Delta r_c}, \quad (8)$$

which characterizes advection of colloidal particles relative to diffusion. Free particles near the surface of a cluster will exhibit a velocity $\mathcal{O}(U_0)$ relative to the aggregate. For δ in this regime, Pe is $\mathcal{O}(10^2)$. Thus, once shear has loosened the more weakly coordinated surface particles, advection denies them sufficient time to relax to the crystalline minimum energy state. Based upon this mechanism, we hypothesize that the nonuniform shear also causes a dependence of the shear-induced melting on the channel width, where wider channels require a stronger global shear strength to fully melt colloidal aggregates. Indeed, setting the threshold for full melting at $f_{\text{crystal}}(\delta_c) = 1\%$, we find

that δ_c increases with channel width W (inset of Fig. 2). This trend will eventually stop for macroscopic channels, where the shear will be uniform on the scale of the colloidal aggregates. Lastly, we note that crystallization can also be induced by variation of the shear frequency in a system of attractive colloids with oscillatory shear⁴¹ or by shearing purely repulsive colloids at high packing fraction.⁴²

3.3 Rheology and structural evolution

When the flow is strong enough to alter phase behavior at $\delta > 0.3$, the coupling of its nonuniform shear and narrow confinement has a strong effect on the dynamics and structural evolution of colloidal aggregates. This is illustrated by the cross-sectional particle distribution for different channels prior to any substantial crystallization (Fig. 3). In a wider channel, clusters initially are much smaller than the channel width and are pulled away from the channel center by lift forces induced by the nonuniform shear (Fig. 3b). This lateral motion, first observed by Segré and Silberberg,⁴³ has been widely studied in Poiseuille flow at large Reynolds numbers,^{44–46} but recently also has found application in microfluidics⁴⁷ with Reynolds numbers down to $Re = 0.04$. By contrast, in a narrow channel (Fig. 3a) clusters readily reach sizes comparable to the channel cross-section and are pushed back to the center by wall effects. A similar focusing phenomenon, although driven by inertia-elastic effects instead, has also been reported for viscoelastic fluids.⁴⁸ A side effect of the focusing of the colloids is that the geometry of the channel barely affects their behavior. More interestingly, we find that the focusing contributes to a rather remarkable mechanism through which colloidal clusters attain an ordered structure in the phase transition region $1 \lesssim \delta \lesssim 2$.

To illustrate this, Fig. 4 shows the evolution of the system at flow strength $\delta = 1.4$ (marked by the dot-dashed vertical line in Fig. 2). Starting from a random uniform dispersion, colloids aggregate into droplets. These droplets are focused around the centerline and tend to concatenate into threads, provided that the channel is sufficiently narrow, $W \lesssim 10\sigma_c$ (for wider channels, the clusters tend to rotate along the wall). Upon elongation of these threads by the shear flow, they evolve into chains of

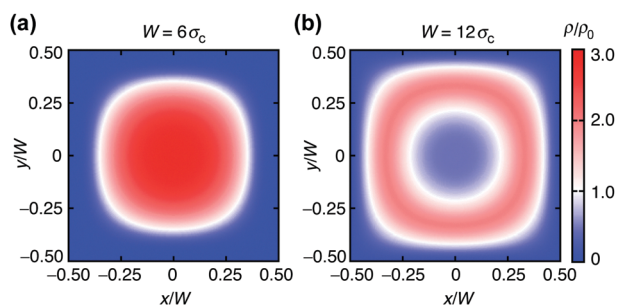


Fig. 3 Particle distribution prior to crystallization. Profiles of local particle density ρ normalized by the global density ρ_0 for two different channel widths $W = 6\sigma_c$ (a) and $W = 12\sigma_c$ (b), respectively. The results are obtained prior to any substantial crystallization and are representative for a wide span of flow strengths with $\delta > 0.3$, corresponding to Reynolds number $Re > 0.22$. The white bands ($\rho = \rho_0$) mark the transition regions from concentrated to depleted domains, relative to the global density.

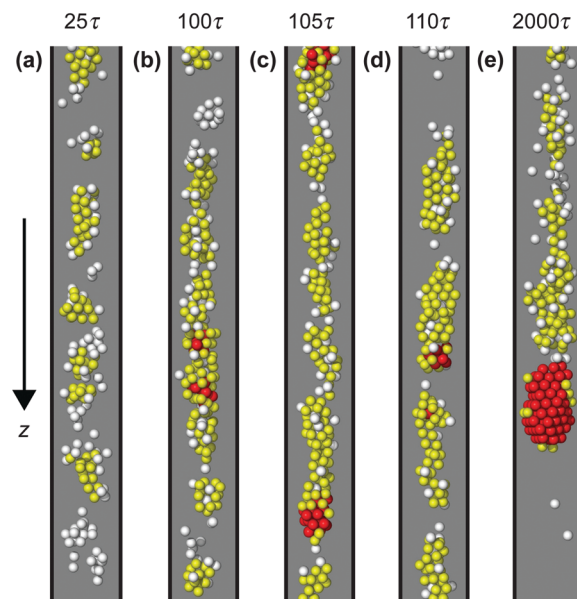


Fig. 4 Evolution of colloidal aggregates under flow. Flow direction is indicated by the arrow, times are marked above the columns. Colloids residing in the gas, liquid, and crystal states are marked in white, yellow, and red, respectively. (a) Initially, the strong attractions cause colloids to aggregate and form droplets. The shear flow elongates these droplets along the channel axis. (b) The relative motion of the droplets causes them to concatenate into a thread structure. (c) As these threads are further elongated, they evolve into a chain of “packets”. (d) The chains of connected packets break up again into droplets, but of more regular shapes. The events in panels (b–d) happen in short order. The pressure gradient is such that a pure fluid system has a fluid flow velocity $U_0 \approx 10.2\sigma_c/\tau$ at the centerline. (e) After tens of break-merge cycles ($t = 2000\tau$ shown here), faceted close-packed crystals arise.

“packets” that then continue to break up into “droplets”. Subsequently, these droplets then merge again into threads. Such break-ups and mergers last for many (20–50) cycles, until close-packed crystals with dimensions up to the size of the channel cross-section emerge and strongly disturb the flow (Movie S1, ESI†). Why and how does the dynamics of aggregates lead to their final crystallization? To answer this question, we need to consider the colloidal dynamics within individual aggregates as well as the collective dynamics of droplets.

Fig. 5 summarizes the rheology of colloidal aggregates before their final crystallization. Clusters experience hydrodynamic flow forces that propel them forward at their center, but exert an oppositely oriented drag at their surfaces. This is illustrated by the sign reversal of $F(r)$, the component of the net hydrodynamic force along the channel axis (solid line in Fig. 5a), which is calculated from the rate of momentum transfer between fluid particles and colloids. Like conventional liquids, clusters continuously deform under shear, as demonstrated by the non-uniform velocity distribution $V(r)$ (dashed line). Interestingly, these liquid-like clusters simultaneously display both dilatant and pseudoplastic behaviors. Fig. 5b shows the dependence of their effective viscosity μ on local shear rate $\dot{\gamma}$. At the surfaces of the cluster, where $\dot{\gamma}$ is large, melting takes place and shear thinning results, with a power-law behavior $\mu \propto \dot{\gamma}^{-0.6}$. In contrast, at the

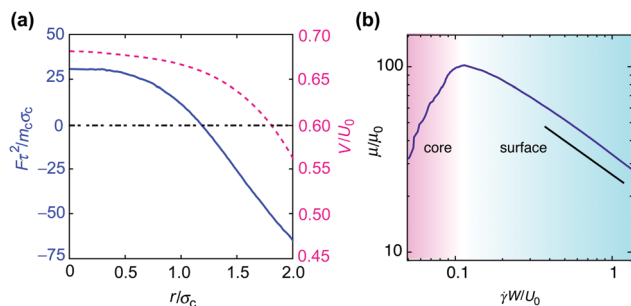


Fig. 5 Rheology of aggregates. (a) Radial distribution of hydrodynamic forces and colloidal velocities. Clusters are deformed by forces $F(r)$ exerted by the fluid, shown here (solid blue curve) as a function of the distance r to the center of the channel. The dotted black line marks $F = 0$ to highlight the sign reversal of the net force. The forces push the aggregate cores (small r) and pull their surfaces (large r). This results in nonuniform colloidal velocities V (dashed pink curve, normalized by the free-channel flow velocity U_0 at the center line). (b) Non-Newtonian properties of colloidal aggregates. Normalized effective viscosity μ of the aggregates is shown as a function of local shear rate $\dot{\gamma} = dV/dr$. The viscosity is calculated as $\mu = \Sigma/\dot{\gamma}$, where Σ is the local shear stress $(1/\sigma_c)dF/dr$. The aggregates undergo shear thickening at their cores (pink-shaded region) with low $\dot{\gamma}$ whereas shear thinning at their surfaces (cyan-shaded region) with high $\dot{\gamma}$. The shear thinning displays a power-law behavior with exponent around -0.6 .

cluster core, where $\dot{\gamma}$ is relatively small, the colloids undergo shear thickening by forming compact microstructures that will initiate crystal nucleation. Although a suspension of attractive colloids typically does not undergo shear thickening,⁴⁹ the induced crystal nuclei here resemble hydroclusters in a suspension of repulsive particles,⁴⁹ which form under large shear and cause common thickening effects.

The shear-induced deformation leads to an increase in surface area that is counteracted by the surface tension Γ arising from interparticle attractions. For water, with $\Gamma \sim 10^{-1} \text{ J m}^{-2}$, this competition results in the Plateau–Rayleigh instability,⁵⁰ breaking up a long thread into droplets. *Via* experiments on falling granular streams it has been demonstrated⁵¹ that for inviscid flow even an extremely small surface tension ($\Gamma \lesssim 10^{-7} \text{ J m}^{-2}$) is enough to induce this instability. Estimating surface tension as $|E_b|/\sigma_c^2$ (see ref. 52), for colloids of size $0.1\text{--}1 \mu\text{m}$ we obtain $\Gamma \sim 10^{-8}\text{--}10^{-6} \text{ J m}^{-2}$, see ref. 53. A difference, however, is that in the system studied here, the colloids are embedded in a significantly more viscous medium than air. Whereas analytical treatment of this case is far more involved (see ref. 54 for an overview of related work in the context of liquid jets embedded in a second liquid), we observe that Rayleigh’s original treatment,⁵⁰ which relies solely on a static description, still applies. Interestingly, for driven colloidal particles, albeit without attraction, the related Rayleigh–Taylor instability has been observed as well.⁵⁵

3.4 Plateau–Rayleigh instability

To verify the mechanism underlying the instability of the colloidal threads, we characterize the geometry of the aggregates both before and after the break-up events. Prior to such an event, the thread exhibits variations in its radius (Fig. 4c). In the Plateau–Rayleigh instability, long-wavelength fluctuations

($kR_0 < 1$, where k is the wave number and R_0 the average thread radius) are unstable due to pressure differences⁵⁶ and cause the thread to break up in individual droplets with characteristic size determined by the fastest-growing wave mode.⁵⁰ For the system examined here, the surface tension driving the break-up of the colloidal threads into clusters arises from the colloidal attractions. To confirm the quantitative applicability of Rayleigh’s argument to the colloidal streams, we extract the elongated threads from the simulations and decompose their radius profile $R(z)$ into wave modes. The resulting spectrum (Fig. 6a) not only confirms that the majority of the wave numbers lie in the regime $kR_0 < 1$, but also shows that the dominant wave number $kR_0 \approx 0.7$ coincides with the well-known dispersion relation,^{50,54} which predicts a maximum at $kR_0 \approx 0.697$. Once the break-up into colloidal aggregates has occurred, we accumulate a joint histogram of their length l and diameter w (Fig. 6b). All cluster aspect ratios obey the stability criterion $l/w < \pi$, demonstrating that all modes with $kR_0 < 1$ indeed have disappeared.

Subsequently, aggregates of different sizes acquire different velocities, as small clusters are mainly transported by the fast flow near the channel center. This causes the small clusters to “catch up” with the large clusters and is responsible for the re-merging into long threads, which restarts the cycle. This cyclic behavior induced by the Plateau–Rayleigh instability relies on the molten surfaces of the aggregates, and terminates when large crystals emerge (Movie S1, ESI†). The number of the cycles is determined by the competition between shear flow and particle attractions. It increases from 0 at $\delta \approx 1$, the onset of surface melting, to infinity at $\delta \approx 2$, where crystals can no longer form.

Thus, the entire process can be summarized as follows: nonuniform shear melts the surface of gel-like clusters but gradually crystallizes their cores. Colloids in the molten surface layer energetically adjust their positions and either join the

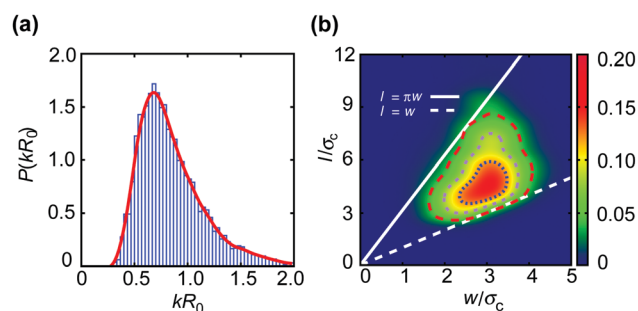


Fig. 6 Plateau–Rayleigh instability. (a) Spectrum reflecting the prevalence of wave numbers in elongated colloidal threads prior to rupture. Notably, the dominant wave number kR_0 (with R_0 the average thread radius) coincides with the fastest growing fluctuation predicted by the Rayleigh dispersion relation. The fitted spline is a guide to the eye. (b) Distribution of cluster widths w and lengths l after break-up, confined by the spherical limit (aspect ratio $l/w = 1$) and the stability criterion $l/w = \pi$. For each cluster, the squared eigenvalues of its gyration tensor are calculated, $\lambda_1^2 \leq \lambda_2^2 \leq \lambda_3^2$. The length and width of the cluster are defined as $l = \sqrt{5\lambda_3^2/3}$ and $w = \sqrt{5(\lambda_1^2 + \lambda_2^2)/6}$. The contour lines (from outer to inner) correspond to probability densities Reaction conditions: 5.0, 0.08 and 0.12, respectively.

crystalline core by forming enough neighbor bonds to resist the shear or simply flow past the core. Owing to the Plateau–Rayleigh instability, these mobile colloids can detach from the crystallized core and be collected in droplets. Thanks to the focusing effects induced by the narrow channel, droplets concatenate and reassemble colloids for further crystal growth. This cyclic process of breaking and merging eventually produces crystals up to the channel size (Fig. 4d), even though global shear is strong enough to disrupt individual colloidal bonds. We find that this picture generally holds as long as the colloidal volume fraction is less than 10%; at higher volume fractions we only observe continuous threads of colloids.

4 Summary

In conclusion, employing molecular dynamics simulations coupled to an explicit hydrodynamic solver, we have examined the phase behavior and dynamics of attractive colloids exposed to shear flow within a microchannel. For moderate flow strengths, the shear aids the colloids in overcoming kinetic arrest, thereby enhancing the crystalline order of the aggregates. Conversely, high shear strengths completely disrupt the colloidal ordering. Strikingly, in the transition regime a cyclic effect that relies on a combination of nonuniform shear and the Plateau–Rayleigh instability results in large crystalline aggregates.

These findings should be testable in microfluidic experiments. One could pump a dilute suspension of micron-sized colloids through a $\sim 10\ \mu\text{m}$ -wide opening. To introduce an $8k_{\text{B}}T$ attraction, polymers with volume fraction 0.45 and radius of gyration 35 nm would need to be added. Then, upon gradual increase of the pumping pressure, one would observe a transition from shear-induced crystallization to melting at flow speed $U_0 = \mathcal{O}(10^2)\ \mu\text{m s}^{-1}$. Within the transition regime, we predict observation of the cyclic process leading to the final crystallization.

The phase and dynamic behavior of the system can also be altered by varying the colloidal interactions. A decrease of the interaction range Δr_{c} or an increase in the magnitude of the interaction strength ΔE_{b} makes aggregates harder to melt. However, low values of ΔE_{b} result in a weak surface tension, which eventually might suppress the Plateau–Rayleigh instability as well as the cyclic dynamics.

Beyond the fundamental relevance for the fluid mechanics of confined colloidal suspensions, the insights derived from this prototypical system apply to a wide variety of contexts, including the pumping of colloidal inks, microfluidics-based manufacturing set-ups and the capillary flow of aggregating entities in biological systems.

Conflicts of interest

There are no conflicts to declare.

Acknowledgements

This research was supported through award 70NANB14H012 from the U.S. Department of Commerce, National Institute of

Standards and Technology, as part of the Center for Hierarchical Materials Design (CHiMaD) and by the National Science Foundation through Grant No. DMR-1121262 at the Materials Research Center of Northwestern University and DMR-1610796. We gratefully acknowledge access to the Quest high-performance computing facility at Northwestern University.

References

- 1 P. J. Lu, E. Zaccarelli, F. Ciulla, A. B. Schofield, F. Sciortino and D. A. Weitz, Gelation of particles with short-range attraction, *Nature*, 2008, **453**, 499–504.
- 2 P. N. Segrè, V. Prasad, A. B. Schofield and D. A. Weitz, Glasslike kinetic arrest at the colloidal-gelation transition, *Phys. Rev. Lett.*, 2001, **86**, 6042–6045.
- 3 A. I. Campbell, V. J. Anderson, J. S. van Duijneveldt and P. Bartlett, Dynamical arrest in attractive colloids: The effect of long-range repulsion, *Phys. Rev. Lett.*, 2005, **94**, 208301.
- 4 F. Sciortino, S. Mossa, E. Zaccarelli and P. Tartaglia, Equilibrium cluster phases and low-density arrested disordered states: The role of short-range attraction and long-range repulsion, *Phys. Rev. Lett.*, 2004, **93**, 055701.
- 5 Q. Wang, L. Wang, M. S. Detamore and C. Berklund, Biodegradable colloidal gels as moldable tissue engineering scaffolds, *Adv. Mater.*, 2008, **20**, 236–239.
- 6 J. E. Smay, J. Cesarano, III and J. A. Lewis, Colloidal inks for directed assembly of 3-D periodic structures, *Langmuir*, 2002, **18**, 5429–5437.
- 7 A. Zaccone, D. Gentili, H. Wu, M. Morbidelli and E. Del Gado, Shear-driven solidification of dilute colloidal suspensions, *Phys. Rev. Lett.*, 2011, **106**, 138301.
- 8 Y. L. Wu, D. Derks, A. van Blaaderen and A. Imhof, Melting and crystallization of colloidal hard-sphere suspensions under shear, *Proc. Natl. Acad. Sci. U. S. A.*, 2009, **106**, 10564–10569.
- 9 M. J. Stevens, M. O. Robbins and J. F. Belak, Shear melting of colloids: A nonequilibrium phase diagram, *Phys. Rev. Lett.*, 1991, **66**, 3004–3007.
- 10 V. Kobelev and K. S. Schweizer, Strain softening, yielding, and shear thinning in glassy colloidal suspensions, *Phys. Rev. E: Stat., Nonlinear, Soft Matter Phys.*, 2005, **71**, 021401.
- 11 X. Cheng, J. H. McCoy, J. N. Israelachvili and I. Cohen, Imaging the microscopic structure of shear thinning and thickening colloidal suspensions, *Science*, 2011, **333**, 1276–1279.
- 12 N. J. Wagner and J. F. Brady, Shear thickening in colloidal dispersions, *Phys. Today*, October 2009, **62**, 27–32.
- 13 J. L. McWhirter, H. Noguchi and G. Gompper, Flow-induced clustering and alignment of vesicles and red blood cells in microcapillaries, *Proc. Natl. Acad. Sci. U. S. A.*, 2009, **106**, 6039–6043.
- 14 P. Calvert, Inkjet printing for materials and devices, *Chem. Mater.*, 2001, **13**, 3299–3305.
- 15 M. H. G. Duits, S. Ghosh and F. Mugele, Measuring advection and diffusion of colloids in shear flow, *Langmuir*, 2015, **31**, 5689–5700.

- 16 S. Ghosh, F. Mugele and M. H. G. Duits, Effects of shear and walls on the diffusion of colloids in microchannels, *Phys. Rev. E: Stat., Nonlinear, Soft Matter Phys.*, 2015, **91**, 052305.
- 17 A. Terray, J. Oakey and D. W. M. Marr, Microfluidic control using colloidal devices, *Science*, 2002, **296**, 1841–1844.
- 18 E. M. Chan, A. P. Alivisatos and R. A. Mathies, High-temperature microfluidic synthesis of CdSe nanocrystals in nanoliter droplets, *J. Am. Chem. Soc.*, 2005, **127**, 13854–13861.
- 19 D. Psaltis, S. R. Quake and C. Yang, Developing optofluidic technology through the fusion of microfluidics and optics, *Nature*, 2006, **442**, 381–386.
- 20 P. Kanehl and H. Stark, Hydrodynamic segregation in a bidisperse colloidal suspension in microchannel flow: A theoretical study, *J. Chem. Phys.*, 2015, **142**, 214901.
- 21 G. Yi, T. Thorsen, V. N. Manoharan, M.-J. Hwang, S.-J. Jeon, D. J. Pine, S. R. Quake and S.-M. Yang, Generation of uniform colloidal assemblies in soft microfluidic devices, *Adv. Mater.*, 2003, **15**, 1300–1304.
- 22 R. F. Shepherd, J. C. Conrad, S. K. Rhodes, D. R. Link, M. Marquez, D. A. Weitz and J. A. Lewis, Microfluidic assembly of homogeneous and Janus colloid-filled hydrogel granules, *Langmuir*, 2006, **22**, 8618–8622.
- 23 S. A. Khan and K. F. Jensen, Microfluidic synthesis of titania shells on colloidal silica, *Adv. Mater.*, 2007, **19**, 2556–2560.
- 24 J. Vermant and M. J. Solomon, Flow-induced structure in colloidal suspensions, *J. Phys.: Condens. Matter*, 2005, **17**, R187–R216.
- 25 P. J. Lu, J. C. Conrad, H. M. Wyss, A. B. Schofield and D. A. Weitz, Fluids of clusters in attractive colloids, *Phys. Rev. Lett.*, 2006, **96**, 028306.
- 26 S. Asakura and F. Oosawa, On interaction between two bodies immersed in a solution of macromolecules, *J. Chem. Phys.*, 1954, **22**, 1255–1256.
- 27 A. M. Puertas, M. Fuchs and M. E. Cates, Simulation study of nonergodicity transitions: Gelation in colloidal systems with short-range attractions, *Phys. Rev. E: Stat., Nonlinear, Soft Matter Phys.*, 2003, **67**, 031406.
- 28 J. K. Whitmer and E. Luijten, Sedimentation of aggregating colloids, *J. Chem. Phys.*, 2010, **134**, 034510.
- 29 M. G. Noro and D. Frenkel, Extended corresponding-states behavior for particles with variable range attractions, *J. Chem. Phys.*, 2000, **113**, 2941–2944.
- 30 G. Gompper, T. Ihle, D. M. Kroll and R. G. Winkler, *Advanced Computer Simulation Approaches for Soft Matter Sciences III*, Springer, Berlin, 2008, vol. 221 of *Advances in Polymer Science*, pp. 1–87.
- 31 J. T. Padding and A. A. Louis, Hydrodynamic interactions and Brownian forces in colloidal suspensions: Coarse-graining over time and length scales, *Phys. Rev. E: Stat., Nonlinear, Soft Matter Phys.*, 2006, **74**, 031402.
- 32 J. K. Whitmer and E. Luijten, Influence of hydrodynamics on cluster formation in colloid-polymer mixtures, *J. Phys. Chem. B*, 2011, **115**, 7294–7300.
- 33 J. K. Whitmer and E. Luijten, Fluid-solid boundary conditions for multiparticle collision dynamics, *J. Phys.: Condens. Matter*, 2010, **22**, 104106.
- 34 F. M. White, *Viscous Fluid Flow*, McGraw-Hill, Boston, 3rd edn, 2006.
- 35 N. A. Mortensen, F. Okkels and H. Bruus, Reexamination of Hagen-Poiseuille flow: Shape dependence of the hydraulic resistance in microchannels, *Phys. Rev. E: Stat., Nonlinear, Soft Matter Phys.*, 2005, **71**, 057301.
- 36 N. Koumakis, E. Moghimi, R. Besseling, W. C. K. Poon, J. F. Brady and G. Petekidis, Tuning colloidal gels by shear, *Soft Matter*, 2015, **11**, 4640–4648.
- 37 N. A. Mahynski, A. Z. Panagiotopoulos, D. Meng and S. K. Kumar, Stabilizing colloidal crystals by leveraging void distributions, *Nat. Commun.*, 2014, **5**, 4472.
- 38 P. J. Steinhardt, D. R. Nelson and M. Ronchetti, Bond-orientational order in liquids and glasses, *Phys. Rev. B: Condens. Matter Mater. Phys.*, 1983, **28**, 784–805.
- 39 W. Lechner and C. Dellago, Accurate determination of crystal structures based on averaged local bond order parameters, *J. Chem. Phys.*, 2008, **129**, 114707.
- 40 A. Fortini, E. Sanz and M. Dijkstra, Crystallization and gelation in colloidal systems with short-ranged attractive interactions, *Phys. Rev. E: Stat., Nonlinear, Soft Matter Phys.*, 2008, **78**, 041402.
- 41 P. A. Smith, G. Petekidis, S. U. Egelhaaf and W. C. K. Poon, Yielding and crystallization of colloidal gels under oscillatory shear, *Phys. Rev. E: Stat., Nonlinear, Soft Matter Phys.*, 2007, **76**, 041402.
- 42 M. Ramaswamy, N. Y. C. Lin, B. D. Leahy, C. Ness, A. M. Fiore, J. W. Swan and I. Cohen, How confinement-induced structures alter the contribution of hydrodynamic and short-ranged repulsion forces to the viscosity of colloidal suspensions, *Phys. Rev. X*, 2017, **7**, 041005.
- 43 G. Segré and A. Silberberg, Radial particle displacements in Poiseuille flow of suspensions, *Nature*, 1961, **189**, 209–210.
- 44 G. Segré and A. Silberberg, Behaviour of macroscopic rigid spheres in Poiseuille flow part 2. Experimental results and interpretation, *J. Fluid Mech.*, 1962, **14**, 136–157.
- 45 B. P. Ho and L. G. Leal, Inertial migration of rigid spheres in two-dimensional unidirectional flows, *J. Fluid Mech.*, 1974, **65**, 365–400.
- 46 J.-P. Matas, J. F. Morris and É. Guazzelli, Inertial migration of rigid spherical particles in Poiseuille flow, *J. Fluid Mech.*, 2004, **515**, 171–195.
- 47 D. Di Carlo, Inertial microfluidics, *Lab Chip*, 2009, **9**, 3038–3046.
- 48 E. J. Lim, T. J. Ober, J. F. Edd, S. P. Desai, D. Neal, K. W. Bong, P. S. Doyle, G. H. McKinley and M. Toner, Inertio-elastic focusing of bioparticles in microchannels at high throughput, *Nat. Commun.*, 2014, **5**, 4120.
- 49 E. Brown and H. M. Jaeger, Shear thickening in concentrated suspensions: phenomenology, mechanisms and relations to jamming, *Rep. Prog. Phys.*, 2014, **77**, 046602.
- 50 Lord Rayleigh, On the instability of jets, *Proc. London Math. Soc.*, 1878, **s1-s10**, 4–13.
- 51 J. R. Royer, D. J. Evans, L. Oyarte, Q. Guo, E. Kapit, M. E. Möbius, S. R. Waitukaitis and H. M. Jaeger, High-speed tracking of rupture and clustering in freely falling granular streams, *Nature*, 2009, **459**, 1110–1113.

- 52 J. N. Israelachvili, *Intermolecular and Surface Forces*, Academic, San Diego, 3rd edn, 2011.
- 53 E. H. A. de Hoog and H. N. W. Lekkerkerker, Measurement of the interfacial tension of a phase-separated colloid-polymer suspension, *J. Phys. Chem. B*, 1999, **103**, 5274–5279.
- 54 J. Eggers and E. Villermaux, Physics of liquid jets, *Rep. Prog. Phys.*, 2008, **71**, 036601.
- 55 A. Wysocki, C. P. Royall, R. G. Winkler, G. Gompper, H. Tanaka, A. van Blaaderen and H. Löwen, Direct observation of hydrodynamic instabilities in a driven non-uniform colloidal dispersion, *Soft Matter*, 2009, **5**, 1340–1344.
- 56 J. Plateau, *Statique Expérimentale et Théorique des Liquides Soumis aux Seules Forces Moléculaires*, Gauthier-Villars, Paris, 1873.